Journal of Solid State Chemistry 182 (2009) 3013–3020

Contents lists available at ScienceDirect

Journal of Solid State Chemistry

journal homepage: www.elsevier.com/locate/jssc

Synthesis, thermal stability and magnetic properties of the $Lu_{1-x}La_xMn_2O_5$ solid solution

C. Ma [a,b], J.-Q. Yan [a], K.W. Dennis [a], R.W. McCallum [a,b], X. Tan [a,b,*]

[a] Division of Materials Science and Engineering, Ames Laboratory, US-DOE, Ames, IA 50011, USA
[b] Department of Materials Science and Engineering, Iowa State University, Ames, IA 50011, USA

ARTICLE INFO

Article history:
Received 13 May 2009
Received in revised form
31 July 2009
Accepted 13 August 2009
Available online 19 August 2009

Keywords:
Multiferroic
$Lu_{1-x}La_xMn_2O_5$
Thermal decomposition
Magnetic properties

ABSTRACT

Polycrystalline samples of the $Lu_{1-x}La_xMn_2O_5$ solid solution system were synthesized under moderate conditions for compositions with x up to 0.815. Due to the large difference in ionic size between Lu^{3+} and La^{3+}, significant changes in lattice parameters and severe lattice strains are present in the solid solution. This in turn leads to the composition dependent thermal stability and magnetic properties. It is found that the solid solution samples with $x \leq 0.487$ decompose at a single well defined temperature, while those with $x \geq 0.634$ decompose over a temperature range with the formation of intermediate phases. For the samples with $x \leq 0.487$, the primary magnetic transition occurs below 40 K, similar to $LuMn_2O_5$ and other individual RMn_2O_5 (R = Bi, Y, and rare earth) compounds. In contrast, a magnetic phase with a ~200 K onset transition temperature is dominant in the samples with $x \geq 0.634$.

1. Introduction

Multiferroic materials have attracted extensive research interest in recent years due to their coupled ferroic orders in a single phase [1–4]. RMn_2O_5 (R = Bi, Y, and rare earth) is one of the few systems displaying coupled magnetic and ferroelectric properties [5–8]. The RMn_2O_5 compounds crystallize in an orthorhombic structure with the space group *Pbam*. In the crystal lattice, R^{3+} ions are coordinated with eight oxygen atoms in RO_8 scalenohedra, and infinite chains of edge-sharing $Mn^{4+}O_6$ octahedra running along the c axis are interconnected by the $Mn^{3+}O_5$ pyramids and RO_8 scalenohedra [9,10]. Most of the RMn_2O_5 compounds are reported to undergo two antiferromagnetic transitions at ~40 and ~20 K, and two ferroelectric transitions at coincident temperatures [5–8]. It is believed that the ferroelectricity in RMn_2O_5 is resulted from the competing magnetic interactions between Mn ions, which are dictated by the Mn–O bond length and the Mn–O–Mn bond angles in the crystal structure [11–15]. As a result of the intimate correlation between magnetic and ferroelectric properties, RMn_2O_5 displays an extremely strong magnetoelectric coupling effect [16,17].

Nonmagnetic R^{3+} ion influences the magnetic behavior of RMn_2O_5 by changing the Mn–O bond length and the Mn–O–Mn bond angles due to the size difference between R^{3+} ions and RO_8 scalenohedra [9,10,18]. Such an ionic size effect makes $LaMn_2O_5$ unique in the RMn_2O_5 family in terms of both structure and magnetic properties. Structurally, $LaMn_2O_5$ is the only one that is thermodynamically unstable at ambient conditions. The La^{3+} ion seems too large to fit the RO_8 scalenohedron and the severe lattice distortion destabilizes the structure [9]. As a consequence, synthesis of $LaMn_2O_5$ requires extreme conditions. For example, an oxygen pressure of 200 bar at 1273 K was used in the previous reports by other researchers [9,10,19]. In contrast, other RMn_2O_5 compounds are stable and can be synthesized under moderate conditions, especially those with the R^{3+} ionic size in the intermediate range. These cations (Eu^{3+}, Gd^{3+}, Tb^{3+}, Dy^{3+} and Ho^{3+}) appear to have the best fit for the RO_8 scalenohedra and the least lattice distortion in RMn_2O_5, as demonstrated by the highest thermal decomposition temperature of the corresponding compounds in the RMn_2O_5 family [20–26]. In terms of magnetic properties, $LaMn_2O_5$ is the only RMn_2O_5 compound possessing a unique magnetic phase with a high onset transition temperature of ~200 K, while the highest reported magnetic transition temperature in other RMn_2O_5 compounds is below 50 K [9]. This unique magnetic phase is of particular interest because the understanding of its nature might provide a means to overcome the disadvantage of the low ordering temperature in the RMn_2O_5 family. It was suggested that the structural distortion caused by the large ionic radius of La^{3+} is responsible for the presence of the high temperature magnetic phase with the ~200 K onset [9].

In order to investigate the nature of the unique magnetic phase of $LaMn_2O_5$, it is critical to study how it is influenced by certain key structural features and the related structural stability caused

* Corresponding author at: Department of Materials Science and Engineering, Iowa State University, Ames, IA 50011, USA. Fax: +1 515 294 5444.
E-mail address: xtan@iastate.edu (X. Tan).

0022-4596/$ - see front matter © 2009 Elsevier Inc. All rights reserved.
doi:10.1016/j.jssc.2009.08.015

by different R^{3+} ionic size. However, this is hard to achieve by simply comparing $LaMn_2O_5$ with other individual RMn_2O_5. First, $LaMn_2O_5$ is the only compound in the RMn_2O_5 family that displays the magnetic phase with ~200 K onset transition temperature, but its synthesis is not a trivial task [9]. Secondly, the number of 4*f* electrons and unpaired electrons, in addition to the size of R^{3+} ions, were also proposed to influence stability of individual RMn_2O_5 compounds [20]. Thirdly, most R^{3+} ions are magnetic and the exchange interactions between R^{3+} and Mn ions, which does not exist in $LaMn_2O_5$, complicate the study of R^{3+} size effect on magnetic properties [27].

In view of these concerns, the solid solution between $LaMn_2O_5$ and another RMn_2O_5 compound with nonmagnetic R^{3+} ions, e.g. $LuMn_2O_5$, would facilitate the study of R^{3+} ionic size effect on the magnetic phase with ~200 K onset transition temperature. In such a solid solution, the effective average R^{3+} ionic size can be freely tuned through adjusting the composition, making it possible to vary the structure features without complications from the *R*–Mn exchange interactions. In addition, substituting the large La^{3+} with a smaller R^{3+} in the solid solution is expected to stabilize the crystal structure and ease the synthesis. However, to the best of our knowledge, only $Ho_{1-x}La_xMn_2O_5$ solid solution with a narrow composition range ($0 \le x \le 0.20$) has been studied previously [28]. In the present work, we successfully synthesized ceramic samples in the $Lu_{1-x}La_xMn_2O_5$ solid solution over a wide composition range of $0 \le x \le 0.815$, corresponding to a range of 0.977–1.126 Å for the effective average R^{3+} ionic radius which is calculated as $(1-x)r_{Lu3+}+xr_{La3+}$. Compared to the 200 bar oxygen pressure required to synthesize pure $LaMn_2O_5$ [9], a moderate condition of 10 bar oxygen pressure at 1273 K was used for the $Lu_{1-x}La_xMn_2O_5$ solid solution. Furthermore, the magnetic phase with ~200 K onset transition temperature, which has been observed in $LaMn_2O_5$, is also present in La-rich samples.

2. Experimental

Single-phase $Lu_{1-x}La_xMn_2O_5$ solid solution samples were prepared by a modified Pechini's method, using high purity La_2O_3 (99.99 wt%), Lu_2O_3 (99.99 wt%), and MnO_2 (99.9 wt%) as raw materials. The compositions we selected for study are $x = 0$, 0.273, 0.487, 0.634, 0.722, and 0.815, whose effective average ionic radii, calculated as $(1-x)r_{Lu3+}+xr_{La3+}$, corresponds to the ionic radius of Lu^{3+}, Dy^{3+}, Eu^{3+}, Pm^{3+}, Nd^{3+}, and Pr^{3+}, respectively. In order to insure proper stoichiometry, powders of La_2O_3 and Lu_2O_3 were dried at 1273 K in air for 15 h and weighed immediately after drying. Appropriate amounts of Lu_2O_3, La_2O_3 and MnO_2 were dissolved in 15 mol/L nitric acid. When dissolving MnO_2, 30% H_2O_2 solution was added in drops until dissolution was complete. Citric acid solution was then added to chelate the metallic ions. The molar ratio of citric acid to total metallic ions was 1.5:1. The pH value of the chelated complex solution was adjusted to 5 by addition of aqueous ammonia solution. The clear solution was dried at 423 K for 12 h and then heated at 873 K for another 12 h in air to form the precursor powder. The precursor powder was uniaxially pressed into pellets and then calcined at 1273 K for 30 h under 10 bar of oxygen to form the phase-pure $Lu_{1-x}La_xMn_2O_5$ ceramic samples.

X-ray powder diffraction was performed on a PANalytical X'pert PRO MPD X-ray diffractometer with monochromatic Cu*K*α radiation at room temperature by step scanning in the angle range $10^\circ \le 2\theta \le 80^\circ$ with increments of 0.02° and dwell time of 300 s. Silicon powder was added to each sample as an internal standard and the Rietveld refinement was performed with the General Structure Analysis System (GSAS) software [29]. The final average *R*-factor is $Rwp = 6.97\%$ with an average $\chi^2 \sim 2.48$. Differential scanning calorimetry (DSC) and thermogravimetric analysis (TGA) measurements were performed using a NETZSCH STA409 Luxx simultaneous DSC/TGA system with a heating rate of 10 K/min in flowing dry air. The TGA results indicate that the weight losses per mole of sample of all the compositions are the same after the high temperature decomposition, which yields the same three solid phases and oxygen for all the $Lu_{1-x}La_xMn_2O_5$ solid solutions (will be discussed in Section 3.2). The uniform weight loss suggests the oxygen content of the $Lu_{1-x}La_xMn_2O_5$ is the same for all samples. The magnetic characterization was carried out with a SQUID (Quantum Design, MPMS).

3. Results and discussion

3.1. Structural study

All the as-calcined solid solution ceramic samples were found to be single phase with the orthorhombic *Pbam* space group, isostructural to the individual RMn_2O_5 compounds. No additional diffraction peaks which could indicate the presence of superstructures or impurity phases were observed from the X-ray diffraction patterns. Fig. 1 shows a representative diffraction spectrum from the composition with $x = 0.815$. We attempted the synthesis of $LaMn_2O_5$ with our approach but failed: no $LaMn_2O_5$ phase was detected in the X-ray diffraction pattern. The results indicate that the unstable $LaMn_2O_5$ can be stabilized through a small fraction substitution of the large La^{3+} ions with smaller Lu^{3+} ions. Clearly the $Lu_{1-x}La_xMn_2O_5$ solid solution ceramics can be synthesized under moderate conditions, compared to the requirement of high oxygen pressure for the synthesis of $LaMn_2O_5$ [15].

The lattice parameters of the solid solution ceramics obtained from Rietveld refinement of the X-ray diffraction pattern are plotted in Fig. 2 as a function of the effective average ionic radius. For comparison, the lattice parameters of individual RMn_2O_5 compounds reported in literature are also displayed [9,23,30]. The lattice parameters *a*, *b* and unit cell volume *V* for the $Lu_{1-x}La_xMn_2O_5$ solid solution are very close to those of their corresponding individual RMn_2O_5 compounds and increase almost linearly with increasing effective average ionic radius, $(1-x)r_{Lu3+}+xr_{La3+}$. However, the lattice parameter *c* of the solid

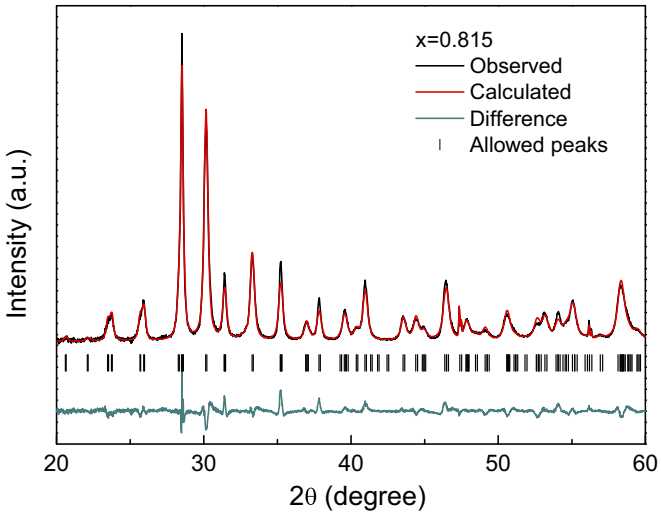

Fig. 1. Refined X-ray diffraction pattern of the $Lu_{0.185}La_{0.815}Mn_2O_5$ solid solution sample. Only the angle range of $20^\circ \le 2\theta \le 60^\circ$ is shown for clarity although a wider angle range of $10^\circ \le 2\theta \le 80^\circ$ is taken and used for refinement.

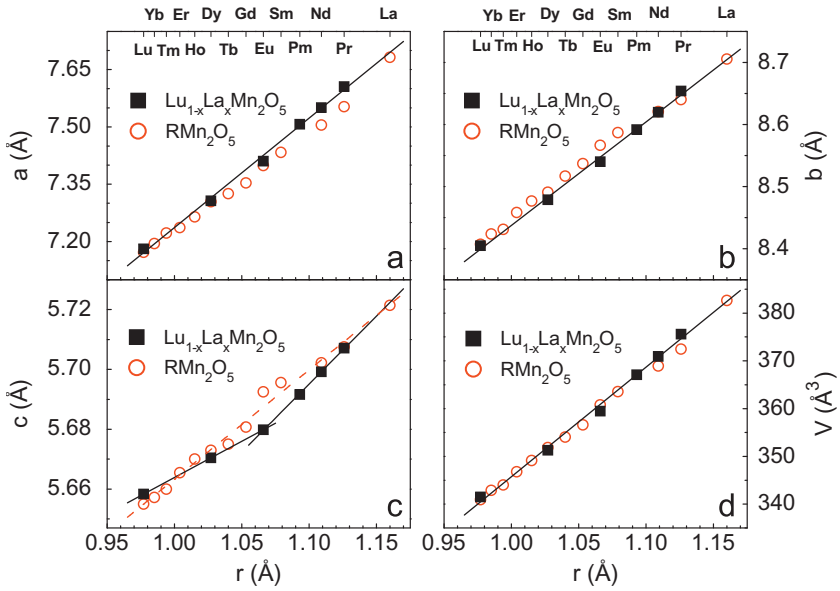

Fig. 2. The lattice parameters and unit cell volume of the $Lu_{1-x}La_xMn_2O_5$ solid solutions as a function of effective average ionic radius of R^{3+}, calculated as $(1-x)r_{Lu3+}+xr_{La3+}$. Data for individual RMn_2O_5 compounds from Refs. [9,23,30] are also shown for comparison. The ionic radius data for R^{3+} under coordination number of eight are taken from Ref. [31]. The lines are drawn as guide for the eyes.

solution does not quite follow the trend of individual RMn_2O_5 compounds, especially for compositions in the intermediate region. It should be noted that the lattice parameter a is the most responsive, while the lattice parameter c is the least responsive, to the change in effective average ionic radius of R^{3+} in the $Lu_{1-x}La_xMn_2O_5$ solid solution. From $LuMn_2O_5$ to $Lu_{0.185}La_{0.815}Mn_2O_5$, the 15.3% increase in the effective average ionic radius of R^{3+} leads to an increase of 5.91% in the lattice parameter a and 0.86% in the lattice parameter c.

In addition to the fit between the R^{3+} (Lu^{3+} or La^{3+}) ion and the RO_8 scalenohedra, the size difference between Lu^{3+} and La^{3+} is also expected to generate local crystal lattice distortion in the $Lu_{1-x}La_xMn_2O_5$ solid solution. For the coordination number of eight in the RMn_2O_5 crystal, La^{3+} is 18.7% larger than Lu^{3+} [31]. Obviously, the size mismatch between Lu^{3+} and La^{3+} is unique to the solid solution and is not present in individual RMn_2O_5 compounds. The lattice distortion resulting from both types of size mismatch (R^{3+}/lattice site, Lu^{3+}/La^{3+}) is expected to be observed in the X-ray diffraction patterns. Indeed, compared to the $LuMn_2O_5$ ($x=0$) sample, significant peak broadening was observed in the X-ray diffraction spectra of $Lu_{1-x}La_xMn_2O_5$ samples with $x=0.273$, 0.487, 0.634, 0.722, and 0.815. As scanning electron microscopy examination of the samples (not shown here) indicated an average grain size of 0.3–0.5 μm in the as-calcined ceramic pellets, we attribute the peak broadening to local lattice distortion, which can be evaluated by the Lorentzian strain parameter LY in the GSAS program [29]:

$$s = 100\% \frac{\pi}{18000} LY \quad (1)$$

where s is the lattice strain, and LY is the refined Lorentzian strain parameter in the GSAS software. In the refinement, the Lorentzian particle size parameter (LX parameter in the GSAS program) was fixed at 0 and the Gaussian width (GW parameter in the GSAS program) was fixed at an average value [29]. The result is displayed in Fig. 3 for the $Lu_{1-x}La_xMn_2O_5$ solid solution as a function of composition x. Compared to $LuMn_2O_5$, the lattice strain in the solid solution increases significantly and peaks at the composition of $x=0.722$.

The lattice strain calculated from X-ray diffraction peak broadening quantitatively reveals the total local lattice distortion

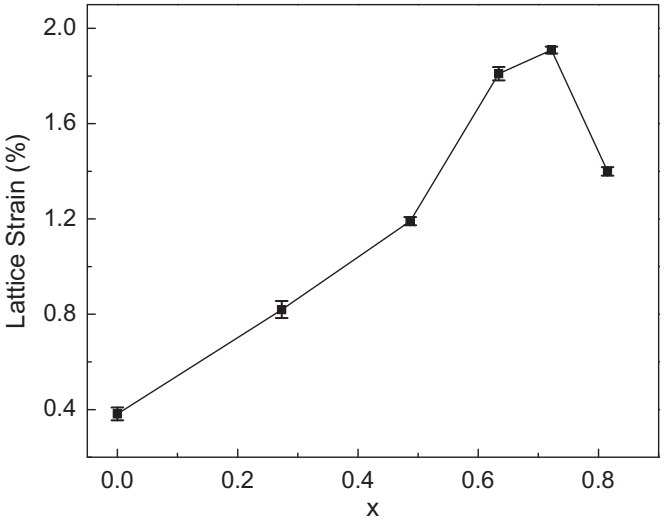

Fig. 3. The lattice strain in the $Lu_{1-x}La_xMn_2O_5$ solid solution calculated from the Rietveld refinement result of X-ray diffraction pattern using the GSAS program.

resulted from both the size mismatch between La^{3+} and Lu^{3+}, and that between the ionic size of R^{3+} and the RO_8 scalenohedra. The contribution from Lu^{3+}/La^{3+} size mismatch should vanish for $x=1$ or 0 and maximize at $x\sim0.5$. However, the maximum lattice strain calculated from the X-ray peak broadening is shifted to the La-rich side at $x=0.722$ (Fig. 3). This implies that La^{3+} generates more severe lattice distortion due to the R^{3+}/RO_8 size mismatch than Lu^{3+}. This speculation is supported by the fact that phase-pure $LuMn_2O_5$ can be prepared under 10 bar O_2 but the formation of $LaMn_2O_5$ requires much more stringent conditions.

3.2. Thermal stability

In addition to the lattice strain calculated from X-ray diffraction patterns, we argue that the local lattice distortion can also be indicated, although indirectly, by thermal stability of the $Lu_{1-x}La_xMn_2O_5$ solid solution. The thermal stability of all the

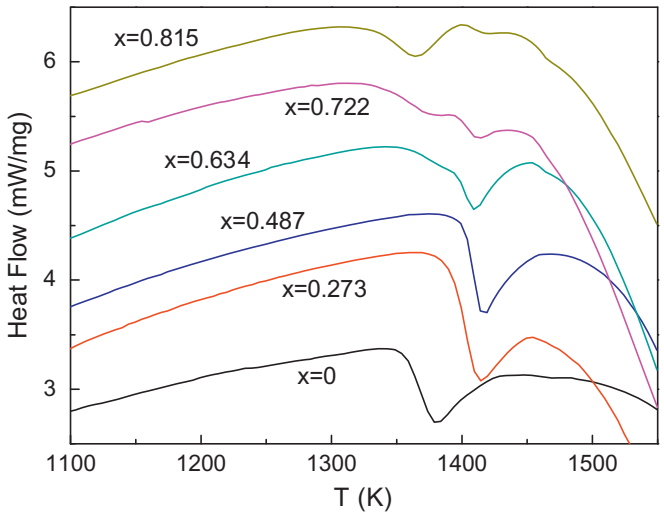

Fig. 4. The DSC curves of all the $Lu_{1-x}La_xMn_2O_5$ solid solution samples revealing the thermal decomposition process. Curves for different x are vertically shifted for clarification.

compositions was evaluated with DSC in flowing dry air and the results are displayed in Fig. 4. For samples with $x \leq 0.487$, only one peak is observed. The onset temperature of this peak increases with increasing x. In contrast, a shoulder appears at the low temperature side of this DSC peak for samples with $x \geq 0.634$. This shoulder becomes more prominent with increasing x and eventually evolves into a major peak in the sample with $x = 0.815$. The X-ray diffraction patterns (not shown here) of the samples annealed at 1523 K (well above all observed DSC anomaly temperatures) for 10 h in air confirmed that the final decomposition products are the same for all compositions: Mn_3O_4, hexagonal $LuMnO_3$, and a monoclinic phase which appears to be nonstoichiometric $LaMnO_3$ (not present in the decomposition products of $LuMn_2O_5$) [32]. Thus, unlike samples with $x \leq 0.487$ which decompose completely within a very narrow temperature range, the samples with $x \geq 0.634$ undergo an additional intermediate step before decomposing completely into these three phases.

The composition $x = 0.722$ was selected to study the intermediate decomposition step. Four samples were heat treated in the DSC. As before, the atmosphere was dry air and the heating rate was 10 K/min. After reaching the maximum temperature, the samples were cooled to room temperature at the fastest rate of the instrument (~40 K/min). The maximum temperatures for the four samples were chosen as 1363, 1378, 1388 and 1395 K, respectively. As expected, equilibrium was not obtained in any of these samples. There is a systematic decrease in the initial material as the maximum temperature of the heat treatment increases. These four heat treatments are denoted as A, B, C and D, respectively (Fig. 5a). A separate sample was annealed at 1353 K for 10 h in the DSC instrument to yield the equilibrium phase distribution prior to the high-temperature DSC anomaly (denoted as E in Fig. 5a).

X-ray powder diffraction of these heat treated samples (Fig. 5b) details the decomposition of the starting material. As the initial $Lu_{1-x}La_xMn_2O_5$ phase (I-125) decomposes, an additional $Lu_{1-x}La_xMn_2O_5$ phase (F-125) with different lattice parameters develops. This is accompanied by the emergence of a monoclinic nonstoichiometric $LaMnO_3$ phase and Mn_3O_4. At equilibrium (E of Fig. 5a), the I-125 phase has disappeared leaving the F-125, the monoclinic nonstoichiometric $LaMnO_3$, and Mn_3O_4. Note that $LuMnO_3$, which has a different structure from $LaMnO_3$,

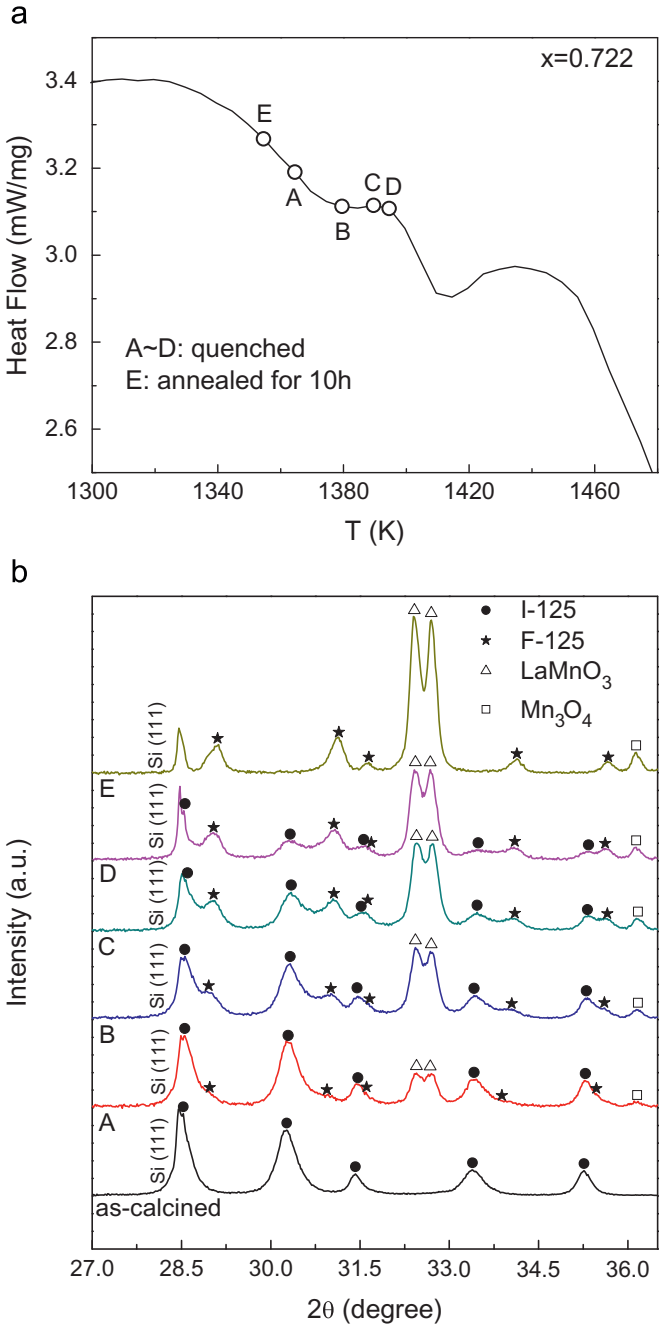

Fig. 5. (a) The DSC curve of the $Lu_{0.278}La_{0.722}Mn_2O_5$ sample with the heat treatment conditions marked; (b) X-ray diffraction patterns of the $Lu_{0.278}La_{0.722}Mn_2O_5$ samples after different heat treatments. The pattern for the as-calcined sample is included for reference.

is not detected in the decomposition product, and from the lattice parameters it appears that there is very little, if any, Lu dissolved in the $LaMnO_3$.

With Si internal standard, the lattice parameters of both I-125 and F-125 were determined from X-ray diffraction patterns for the heat treated $x = 0.722$ samples (Table 1). Since the lattice parameter a is most sensitive to and displays good linearity with the composition of the solid solution (Fig. 2a), it was used to estimate La content in I-125 and F-125. As listed in Table 2, the difference between the lattice parameters of the I-125 and F-125 phases indicates a lower La content in the F-125. In addition, it is evident that La content x decreases for both I-125 and F-125 as the intermediate decomposition proceeds.

Table 1
Lattice parameters of the two $Lu_{1-x}La_xMn_2O_5$ phases in the $x = 0.722$ sample after different heat treatments.

Treatment condition	a (Å)		b (Å)		c (Å)	
	I-125	F-125	I-125	F-125	I-125	F-125
A	7.553(1)	7.437(2)	8.622(1)	8.553(4)	5.696(2)	5.718(3)
B	7.544(2)	7.332(3)	8.617(3)	8.508(2)	5.695(1)	5.678(2)
C	7.533(2)	7.304(1)	8.618(1)	8.489(1)	5.696(3)	5.673(2)
D	7.519(1)	7.291(2)	8.593(1)	8.472(2)	5.688(1)	5.667(2)
E	–	7.2779(8)	–	8.4684(8)	–	5.6651(5)

Table 2
Compositions of the two $Lu_{1-x}La_xMn_2O_5$ phases in the $x = 0.722$ sample after different heat treatments.

Treatment condition	x	
	I-125	F-125
A	0.721	0.500
B	0.705	0.302
C	0.683	0.248
D	0.658	0.225
E	–	0.199

The high-temperature DSC peak in the La-rich compositions ($x = 0.634$, 0.722, and 0.815) corresponds to the decomposition of the La-depleted F-125 composition produced in the intermediate temperature range. It is also noted that the high-temperature DSC anomaly occurs at almost the same temperature for $x = 0.634$, 0.722 and 0.815 (Fig. 4), which indicates that the F-125 phase at the end of the intermediate step might have similar La-content for these three samples. This is indeed the case. Additional samples of $x = 0.634$ and 0.815 were treated under condition E (annealing at 1353 K in air for 10 h) to yield the equilibrium phases of the intermediate decomposition step. The La-content of the F-125 phase was calculated from the a lattice parameter to be 0.189, 0.199, 0.178 for the samples of $x = 0.634$, 0.722, 0.815, respectively.

The thermal stability results are summarized in Fig. 6 where the thermal decomposition temperature of the $Lu_{1-x}La_xMn_2O_5$ solid solution is plotted against the effective average ionic radius of R^{3+}. The onset of the only DSC anomaly is taken as the decomposition temperature for samples with $x \leq 0.487$, while the onset of the low-temperature DSC anomaly is considered as the decomposition temperature for samples with $x \geq 0.634$. The previously reported thermal decomposition temperature for individual RMn_2O_5 compounds is also plotted for comparison [20,23]. Note that our measurement indicates a decomposition temperature for $LuMn_2O_5$ ~70 K higher than the literature data. The discrepancy could be attributed to the different measurement conditions and techniques. Despite the discrepancy, Fig. 6 clearly demonstrates that the decomposition temperature of the $Lu_{1-x}La_xMn_2O_5$ solid solution ($x = 0.273$, 0.487, 0.634, 0.722, 0.815) is lower than that of the corresponding individual RMn_2O_5 compounds. The lower thermal stability of $Lu_{1-x}La_xMn_2O_5$ is suggested to be caused by more severe local lattice distortion due to the Lu^{3+}/La^{3+} size mismatch which is not present in individual RMn_2O_5 compounds. In addition, Fig. 6 indicates that the decomposition temperature of the solid solution displays a trend similar to that of individual RMn_2O_5 compounds: The composition with an intermediate ionic size of R^{3+} (1.02 Å $\leq r \leq$ 1.06 Å) is most stable. The results seem to suggest that the effective average radius of R^{3+} is dominant in determining the thermal stability of the $Lu_{1-x}La_xMn_2O_5$ solid solution.

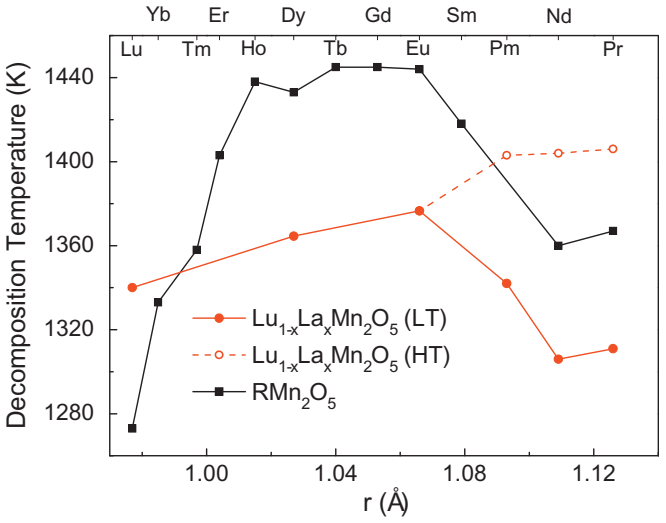

Fig. 6. The decomposition temperature of the $Lu_{1-x}La_xMn_2O_5$ solid solution determined from the DSC curves plotted against the effective average ionic radius $(1-x)r_{Lu3+}+xr_{La3+}$. The high-temperature (HT) DSC peak in the La-rich compositions ($x = 0.634$, 0.722, 0.815) is shown as open circles connected with dashed lines while onset of the low-temperature (LT) DSC peak for La-rich compositions and that of the only DSC peak for Lu-rich compositions ($x = 0$, 0.273, and 0.487) are shown as solid circles. The data for individual RMn_2O_5 compounds taken from Refs. [20,23] are shown for comparison.

3.3. Magnetic properties

Previous researchers reported a magnetic transition with the onset temperature of ~200 K in $LaMn_2O_5$ [9,19]. Under the same measurement condition ($H = 1$ kOe), this transition was observed in the solid solution sample $Lu_{0.185}La_{0.815}Mn_2O_5$, as displayed in Fig. 7. An anomaly appears at ~200 K and the susceptibility increases gradually with decreasing temperature. A small slope change is seen at ~20 K in $Lu_{0.185}La_{0.815}Mn_2O_5$ (Fig. 7), which is different from that reported for $LaMn_2O_5$ where it occurs at ~50 K [19]. In order to verify the ~200 K magnetic transition is from the $Lu_{0.185}La_{0.815}Mn_2O_5$ phase rather than a minor ferromagnetic impurity phase, the possible magnetic impurities Mn–O binaries, La–Mn–O ternaries and Lu–Mn–O ternaries were investigated. To the best of our knowledge, the only compound that might display a high magnetic transition temperature (~200 K) is $LaMnO_{3+\delta}$ [33,34]. To rule out the contribution from this impurity, we prepared $LaMnO_{3+\delta}$ under the conditions used here and investigated its magnetic properties. The magnetic measurements on these $LaMnO_{3+\delta}$ samples revealed an onset transition temperature of ~150 K, well below ~200 K.

Fig. 8 displays the temperature dependence of the magnetization curves of $Lu_{1-x}La_xMn_2O_5$ solid solution samples measured with field cool (FC) and zero field cool (ZFC) modes under an applied field of 100 Oe. The magnetization displays very similar behavior for all the La-rich samples ($x = 0.634$, 0.722, and

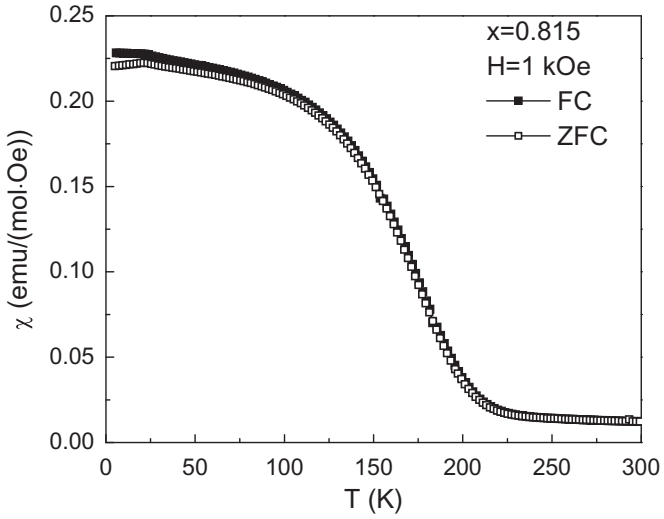

Fig. 7. Susceptibility vs. temperature curve of the $Lu_{0.185}La_{0.815}Mn_2O_5$ sample measured in field cool (FC) and zero field cool (ZFC) modes under an applied field of 1 kOe.

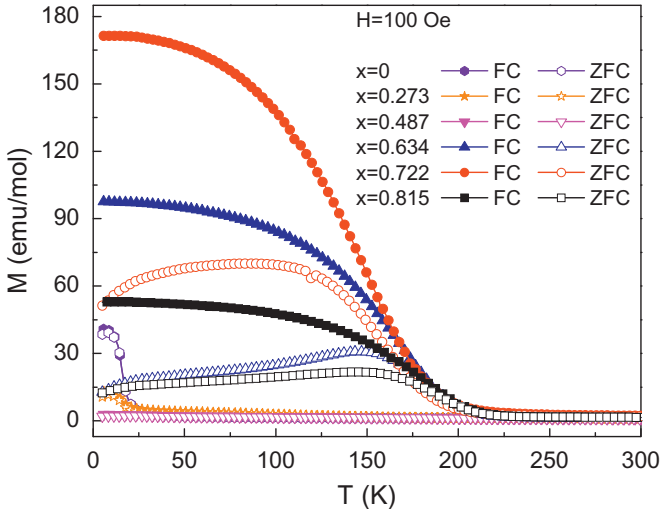

Fig. 8. Magnetization vs. temperature curves of the $Lu_{1-x}La_xMn_2O_5$ samples measured in field cool (FC) and zero field cool (ZFC) modes under an applied field of 100 Oe.

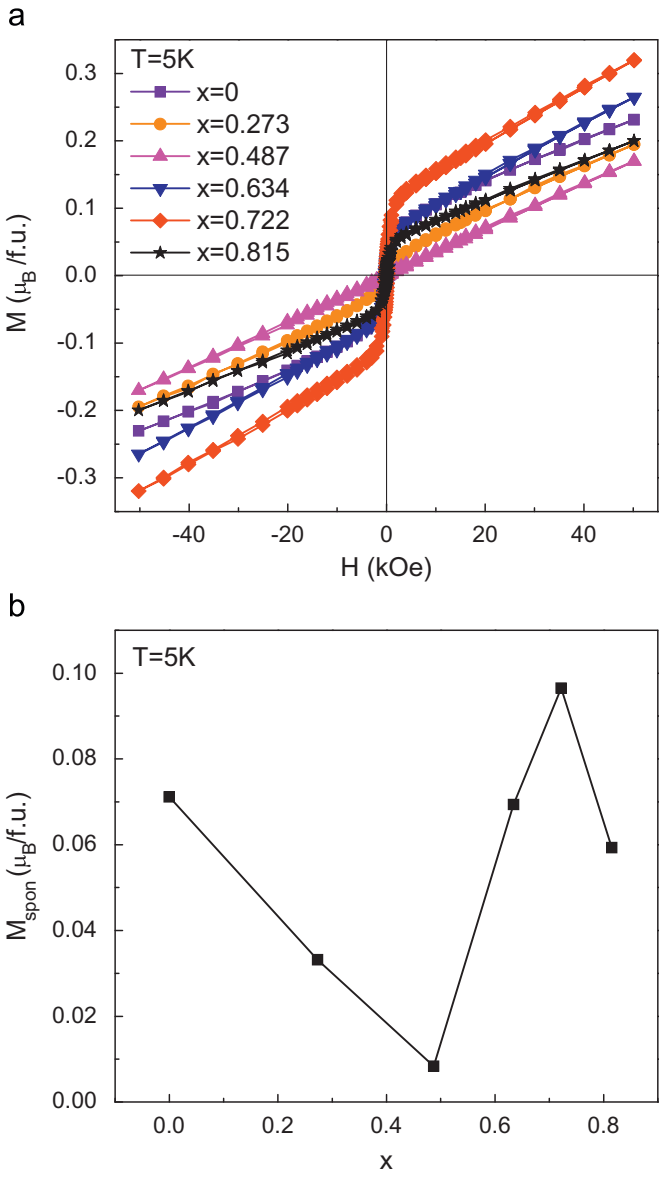

Fig. 9. (a) Magnetization M vs. field H curves of $Lu_{1-x}La_xMn_2O_5$ samples measured at 5 K; (b) the spontaneous moment M_{spon}, which is taken as the zero-field intercept of the linear fit of high-field part ($H > 10$ kOe) of the M vs. H curves, of $Lu_{1-x}La_xMn_2O_5$ samples at 5 K.

0.815): the M vs. T curve is dominated by the anomaly with onset at ~200 K. The magnetization keeps increasing rather gradually as the temperature decreases below 200 K. The bifurcation between the FC and ZFC curves suggests that the magnetic phase with ~200 K onset transition temperature contains a ferromagnetic component. It is noteworthy that the magnitude of the magnetization, especially the magnetization measured with FC mode, follows the decreasing sequence of $x = 0.722$, $x = 0.634$, $x = 0.815$ below 150 K. Similar tendency is also present in the lattice strain (Fig. 3). The Lu-rich samples ($x = 0$, 0.273, and 0.487) display a quite different temperature dependence of magnetization: the dominant anomaly on the magnetization vs. temperature curves is an increase of magnetization with decreasing temperature below ~20 K, while the anomaly with ~200 K onset is barely observable. The bifurcation between the FC and ZFC curves is close to zero.

Fig. 9a displays the magnetization M vs. applied field H curves of $Lu_{1-x}La_xMn_2O_5$ solid solution samples with different compositions measured at 5 K. The M vs. H curves of all the samples display a slope change at ~3 kOe, which indicates a ferromagnetic-like behavior. However, both the coercivity and the remanent magnetization are small for all samples. This type of behavior is characteristic of a nearly compensated antiferromagnet. In this case, the uncompensated moment along the easy axis gives a ferromagnetic-like M vs. H curve which saturates at ~3 kOe, while the high-field part of the M vs. H curve with a linear field dependence is characteristic of the perpendicular susceptibility of an antiferromagnet.

This uncompensated moment, or the spontaneous moment (M_{spon}), can be characterized by the zero-field intercept of the linear fit of the high-field part of the M vs. H curve. Fig. 9b displays the spontaneous moment of $Lu_{1-x}La_xMn_2O_5$ solid solution samples calculated from Fig. 9a. For Lu-rich samples ($x = 0$, 0.273, and 0.487), whose M vs. T curve is dominated by the anomaly with ~20 K onset transition temperature, M_{spon} decreases monotonically with increasing the La content. A sharp increase of the spontaneous moment is observed when La content increases from 0.487 to 0.634, where the dominant magnetic

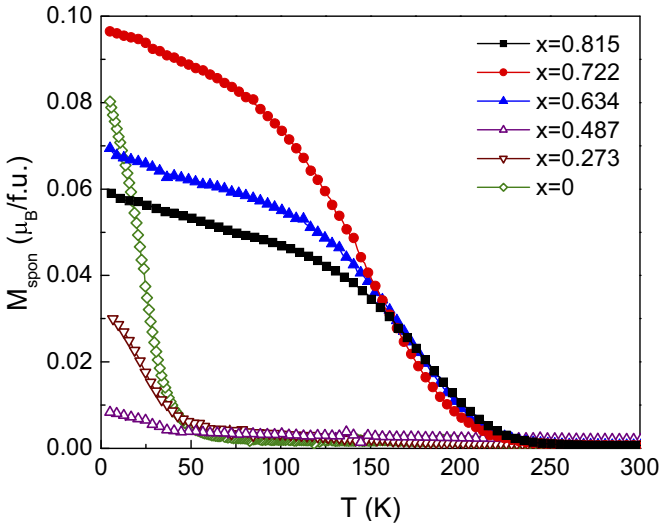

Fig. 10. The temperature dependence of spontaneous moment M_{spon} in the $Lu_{1-x}La_xMn_2O_5$ solid solution samples. M_{spon} is taken as the zero-field intercept of a linear fit of magnetization under applied fields of 10, 20, 30, 40 and 50 kOe.

phase becomes the one with ~200 K onset transition temperature. The spontaneous moment of the La-rich samples ($x = 0.634$, 0.722 and 0.815) takes the decreasing sequence of $x = 0.722$, $x = 0.634$, $x = 0.815$, which resembles the composition dependence of lattice strain (Fig. 3).

Fig. 10 displays M_{spon} as a function of temperature for all the $Lu_{1-x}La_xMn_2O_5$ solid solution samples. The temperature dependence of M_{spon} for La-rich samples ($x = 0.634$, 0.722, and 0.815) is similar to that of magnetization: the M_{spon} vs. T curve is dominated by the anomaly with ~200 K onset. M_{spon} increases with decreasing temperature below ~200 K. Below ~150 K, M_{spon} does not saturate but rather continues to increase with a slightly different slope. In addition, the variation of the magnitude of M_{spon} with La content x follows the same trend as that of lattice strain in a very wide temperature range of $T < \sim 150$ K. For the Lu-rich samples ($x = 0$, 0.273, and 0.487), the ~200 K anomaly can no longer be detected on the M_{spon} vs. T curve, which is consistent with the temperature dependence of magnetization. However, M_{spon} increases sharply with decreasing temperature below ~40 K. The M_{spon} vs. T curve is dominated by this anomaly with ~40 K onset rather than the one with ~20 K onset which dominates the M vs. T curve. A similar behavior has been observed in YMn_2O_5 [35]. YMn_2O_5 orders as 2D incommensurate, 1D incommensurate and commensurate magnetic structure at 45, 40 and 39 K, respectively [5,6]. On further cooling below 20 K, the magnetic structure orders as a low-temperature incommensurate one [5,6]. From this point of view, a similar sequence of magnetic transitions might also take place in Lu-rich ($x = 0$, 0.273, and 0.487) samples. More detailed studies on high quality single crystal samples are necessary to confirm this.

It is noteworthy that the thermal decomposition mechanism (Fig. 4) and the dominant anomaly on the M_{spon} vs. T curve (Fig. 10) in the $Lu_{1-x}La_xMn_2O_5$ solid solution make abrupt changes when the composition x crosses 0.500. In addition, the magnitude of magnetization measured with FC mode under 100 Oe and that of M_{spon} below 150 K with respect to composition x follows the same trend as the lattice strain in La-rich compositions ($x \geq 0.634$). These observations are indications of correlated structural features and the high temperature magnetic phase with ~200 K onset transition temperature.

4. Conclusions

In summary, phase pure $Lu_{1-x}La_xMn_2O_5$ ($0 \leq x \leq 0.815$) solid solution ceramics can be synthesized with a modified Pechini's method under moderate calcination conditions (1273 K, 10 bar O_2). Although the lattice parameters of the solid solution samples are close to those of corresponding individual RMn_2O_5 compounds, severe local lattice distortions are present in the solid solution samples due primarily to the large size difference between Lu^{3+} and La^{3+}. The local lattice distortion not only influences the structural stability (as reflected by the thermal decomposition), but also dictates the magnetic interactions. The magnetic phase with ~200 K onset transition temperature, which was not observed in individual RMn_2O_5 compounds except $LaMn_2O_5$, is present in the La-rich solid solution samples with $x \geq 0.634$. The lattice strain and related structural stability are apparently correlated with the presence of this high temperature magnetic phase. These results suggest that the solid solution approach will be key to studying the dependence of the magnetic behavior of this phase on certain critical structural features and understanding its nature.

Acknowledgment

Ames Laboratory is operated for the US Department of Energy by Iowa State University under Contract No. DE-AC02-07CH11358.

References

[1] T. Kimura, T. Goto, H. Shintani, K. Ishizaka, T. Arima, Y. Tokura, Nature 426 (2003) 55.
[2] R. Ramesh, A. Inam, W.K. Chan, B. Wilkens, K. Myers, K. Remshing, D.L. Hart, J.M. Tarascon, Science 252 (1991) 944.
[3] J. Wang, J.B. Neaton, H. Zheng, V. Nagarajan, S.B. Ogale, B. Liu, D. Viehland, V. Vaithyanathan, D.G. Schlom, U.V. Waghmare, N.A. Spaldin, K.M. Rabe, M. Wuttig, R. Ramesh, Science 299 (2003) 1719.
[4] M. Fiebig, J. Phys. D 38 (2005) R123.
[5] S. Kobayashi, T. Osawa, H. Kimura, Y. Noda, I. Kagomiya, K. Kohn, Jpn. J. Phys. Soc. 73 (2004) 1593.
[6] Y. Noda, H. Kimura, Y. Kamada, Y. Ishikawa, S. Kobayashi, Y. Wakabayashi, H. Sawa, N. Ikeda, K. Kohn, J. Korean Phys. Soc. 51 (2007) 828.
[7] I. Kagomiya, H. Kimura, Y. Noda, K. Kohn, J. Phys. Soc. Jpn. 70 (Suppl. A) (2001) 145.
[8] K. Kohn, Ferroelectrics 162 (1994) 1.
[9] J.A. Alonso, M.T. Casais, M.J. Martínez-Lope, J.L. Martínez, M.T. Fernández-Díaz, J. Phys. Condens. Matter 9 (1997) 8515.
[10] J.A. Alonso, M.T. Casais, M.J. Martínez-Lope, I. Rasines, J. Solid State Chem. 129 (1997) 105.
[11] A.M. Kadomtseva, Y.F. Popov, G.P. Vorobev, K.I. Kamilov, P.N. Makhov, M.M. Tehranchi, A. Phirouznia, Physica B 329 (2003) 856.
[12] L.C. Chapon, P.G. Radaelli, G.R. Blake, S. Park, S.-W. Cheong, Phys. Rev. Lett. 96 (2006) 097601.
[13] Y. Noda, H. Kimura, Y. Kamada, T. Osawa, Physica B 385 (2006) 119.
[14] L.C. Chapon, G.R. Blake, M.J. Gutmann, S. Park, N. Hur, P.G. Radaelli, S.-W. Cheong, Phys. Rev. Lett. 93 (2004) 177402.
[15] G.R. Blake, L.C. Chapon, P.G. Radaelli, S. Park, N. Hur, S.-W. Cheong, J. Rodriguez-Carvajal, Phys. Rev. B 71 (2005) 214402.
[16] W. Prellier, M.P. Singh, P. Murugavel, J. Phys.: Condens. Matter 17 (2005) R803.
[17] D.I. Khomskii, J. Magn. Magn. Mater. 306 (2006) 1.
[18] I. Kagomiya, K. Kohn, Ferroelectrics 219 (1998) 169.
[19] A. Muñoz, J.A. Alonso, M.T. Casais, M.J. Martínez-Lope, J.L. Martínez, M.T. Fernández-Díaz, Eur. J. Inorg. Chem. 4 (2005) 685.
[20] V.F. Balakirev, Y.V. Golikov, Inorg. Mater. 39 (Suppl. 1) (2003) S1.
[21] V.F. Balakirev, Y.V. Golikov, S.G. Titova, O.M. Fedorova, Dokl. Phys. Chem. 388 (2003) 1.
[22] V.F. Balakirev, L.B. Vedmid', A.M. Yankin, Y.V. Golikov, Dokl. Phys. Chem. 389 (2003) 4.
[23] H. Satoh, S. Suzuki, K. Yamamoto, N. Kamegashira, J. Alloys Compd. 234 (1996) 1.
[24] L.B. Vedmid', V.F. Balakirev, A.M. Yankin, Y.V. Golikov, O.M. Fedorova, Glass Phys. Chem. 30 (2004) 345.
[25] Y.V. Golikov, V.F. Balakirev, S.G. Titova, L.B. Vedmid', O.M. Fedorova, Russ. J. Inorg. Chem. 48 (2003) 13.

[26] V.F. Balakirev, L.B. Vedmid', A.M. Yankin, Y.V. Golikov, Dokl. Phys. Chem. 389 (2003) 87.
[27] D. Higashiyama, S. Miyasaka, N. Kida, T. Arima, Y. Tokura, Phys. Rev. B 70 (2004) 174405.
[28] C.C. Yu, S.Y. Huang, C.J. Yeh, C.W. Lee, C.B. Wu, H. Chou, J. Appl. Phys. 103 (2008) 07E310.
[29] A.C. Larson, R.B. Von Dreele, Los Alamos National Laboratory Report LAUR 86 748, 2000.
[30] I. Kagomiya, K. Kohn, T. Uchiyama, Ferroelectrics 280 (2002) 131.
[31] R.D. Shannon, Acta Cryst. A 32 (1976) 751.
[32] A. Maignan, C. Michel, M. Hervieu, B. Raveau, Solid State Commun. 101 (1997) 277.
[33] J. Töpfer, J.C. Grenier, J.P. Doumerc, J. Mater. Chem. 6 (1996) 1511.
[34] J. Töpfer, J.B. Goodenough, J. Solid State Chem. 130 (1997) 117.
[35] C. Ma, J.-Q. Yan, K.W. Dennis, A. Llobet, R.W. McCallum, X. Tan, J. Phys.: Condens. Matter 21 (2009) 346002.